

## **Programmable 3D silk bone marrow niche for platelet generation *ex vivo* and modeling of megakaryopoiesis pathologies**

Christian A. Di Buduo,<sup>1,2</sup> Lindsay S. Wray,<sup>3</sup> Lorenzo Tozzi,<sup>1-3</sup> Alessandro Malara,<sup>1,2</sup> Ying Chen,<sup>3</sup> Chiara E. Ghezzi,<sup>3</sup> Daniel Smoot,<sup>3</sup> Carla Sfara,<sup>4</sup> Antonella Antonelli,<sup>4</sup> Elise Spedden,<sup>5</sup> Giovanna Bruni,<sup>6</sup> Cristian Staii,<sup>5</sup> Luigi De Marco,<sup>7,8</sup> Mauro Magnani,<sup>4</sup> David L. Kaplan,<sup>3\*</sup> Alessandra Balduini<sup>1-3\*</sup>

<sup>1</sup>Department of Molecular Medicine, University of Pavia, Pavia, Italy; <sup>2</sup>Biotechnology Research Laboratories, IRCCS San Matteo Foundation, Pavia, Italy; <sup>3</sup>Department of Biomedical Engineering, Tufts University, Medford, MA, USA; <sup>4</sup>Department of Biomolecular Sciences, Biochemistry and Molecular Biology Section, University of Urbino "Carlo Bo", Urbino, Italy; <sup>5</sup>Department of Physics, Tufts University, Medford, MA, USA; <sup>6</sup>Department of Chemistry, Physical Chemistry Section, University of Pavia, Pavia, Italy; <sup>7</sup>Department of Translational Research, Stem Cells Unit, IRCCS CRO Aviano, Italy; <sup>8</sup>Department of Molecular and Experimental Research, The Scripps Research Institute, La Jolla, CA, USA

\*Correspondence to: Alessandra Balduini ([alessandra.balduini@tufts.edu](mailto:alessandra.balduini@tufts.edu)), David L. Kaplan ([david.kaplan@tufts.edu](mailto:david.kaplan@tufts.edu)), Department of Biomedical Engineering, Tufts University, 4 Colby Street, Medford, MA 02155, USA. Phone: 617-627-2580; Fax:617-627-3231.

C.A.D.B. and L.S.W. contributed equally to this study.

**Short title:** 3D silk bone marrow niche for platelet production

**Scientific category:** Platelets and Thrombopoiesis

## KEY POINTS

- Natural silk protein sponge and vascular tubes reproducing human bone marrow niche environments for functional platelet generation *ex vivo*
- Programmable bioengineered model for the investigation and therapeutic targeting of altered platelet formation

## ABSTRACT

We present a programmable bioengineered three-dimensional silk based bone marrow niche tissue system that successfully mimics the physiology of human bone marrow environment allowing us to manufacture functional human platelets *ex vivo*. Using stem/progenitor cells, megakaryocyte function and platelet generation were recorded in response to variations in extracellular matrix components, surface topography, stiffness, co-culture with endothelial cells and shear forces. Millions of human platelets were produced and showed to be functional based on multiple activation tests. Using adult hematopoietic progenitor cells our system demonstrated the ability to reproduce key steps of thrombopoiesis, including alterations observed in diseased states. A critical feature of the system is the use of natural silk protein biomaterial allowing us to leverage its biocompatibility, non-thrombogenic features, programmable mechanical properties, and surface binding of cytokines, extracellular matrix components and endothelial-derived proteins. This in turn offers new opportunities for the study of blood component production *ex vivo* and provides a superior tissue system for the study of pathologic mechanisms of human platelet production.

## INTRODUCTION

Bone marrow failure is the result of diseases, trauma, or cancer treatments, leading to a decreased production of blood cells and consequent necessity of blood transfusions.<sup>1</sup> There is a critical need for bioengineering models that are able to reproduce key features of the physiological bone marrow environment in order to provide mechanistic understanding and control of hematopoiesis as well as systems for functional blood cell generation and screening of therapeutic compounds *ex vivo*.<sup>2-5</sup>

Bone marrow microenvironment and “niches”, contained in spongy bones, support hematopoietic stem cell self-renewal as well as differentiation into committed lineages in order to support the physiologic homeostasis of blood cells.<sup>6,7</sup> The venous sinusoids are the site of the passage of mature blood cells between the bone marrow compartment and the blood stream. The walls of the sinusoids consist solely of a layer of endothelial cells on a discontinuous basement membrane.<sup>8</sup> Endothelial cells and extracellular matrix components (ECM) components are important for the maintenance of correct hematopoiesis.<sup>9-11</sup> In the bone marrow, platelets are generated by megakaryocytes (Mks) that associate with the bone marrow vasculature where they convert their

cytoplasm into proplatelets that protrude through the vascular endothelium and release platelets into the lumen.<sup>12-14</sup>

In this study, we successfully programmed silk protein biomaterial, a biologically-derived protein polymer with invaluable properties for tissue engineering,<sup>15</sup> to develop an *ex vivo* three-dimensional (3D) tissue model of the bone marrow niche environment in which human Mk function and platelet generation were measured in response to changes in ECM composition, surface topography, stiffness, co-culture with endothelial cells and shear.

## METHODS

### Silk Scaffolds Fabrication

In order to explore the possibility to employ silk as a scaffold for reproducing the physiologic properties of the basement membrane *in vitro*, silk solution (1% w/v), produced by degumming *Bombyx mori* silkworm cocoons,<sup>16</sup> containing polyethylene oxide (PEO) porogen (0.05% w/v; Sigma) was cast on polydimethylsiloxane (PDMS; Dow Corning) molds (45  $\mu\text{L}/\text{cm}^2$  of mold surface area) with different patterns (Table 1) and dried at 22°C for 16 hours.<sup>17</sup> ECM components were added to the silk film, either coated onto the film surface or entrapped within the silk film. The following ECM components were used: 25  $\mu\text{g}/\text{mL}$  type I collagen, 100  $\mu\text{g}/\text{mL}$  fibrinogen, 25  $\mu\text{g}/\text{mL}$  fibronectin, 25  $\mu\text{g}/\text{mL}$  type IV collagen, or 25  $\mu\text{g}/\text{mL}$  laminin. In some experiments silk was mixed with ECM components together with 500 ng/mL vascular cell adhesion molecule-1 (VCAM-1) and 500 ng/mL vascular endothelial growth factor (VEGF). To achieve 'High', 'Medium' and 'Low' silk film mechanical properties samples were water annealed<sup>18</sup> in a vacuum chamber containing 100 mL of water at the bottom of chamber at either 60° for 16 hours or 22°C for 16 hours or 4°C for 6 hours.

Bone marrow microvasculature was mimicked by preparation of gel-spun microtubes.<sup>19</sup> Briefly, 15% aqueous silk solution was mixed with fibronectin, type IV collagen and laminin to a final concentration of 25  $\mu\text{g}/\text{mL}$ , and with 300 ng/mL SDF-1 $\alpha$ . In some experiments the preparation was also mixed with 500 ng/mL vascular cell adhesion molecule-1 (VCAM-1) and 500 ng/mL vascular endothelial growth factor (VEGF). Pores were obtained by adding 6% w/v polyethylene oxide (PEO) to the silk fibroin to a volume ratio of 10:1 silk:PEO. Functionalized silk tubes were trimmed to approximately 1.5 cm in length and secured over the blunt end needles within the perfusion bioreactor chamber.

A porous silk sponge was assembled around the tube using a salt-leaching process.<sup>18</sup> Specifically, a 8% aqueous silk solution was dispensed around the tube and then NaCl particles (approximately 500  $\mu\text{m}$  in diameter) were sifted into the silk solution in a ratio of 1 mL of 8% silk solution to 2 g of NaCl particles. The scaffolds were placed at room temperature for 48 hours and then soaked in distilled water for 48 hours to leach out the NaCl particles.

The Supplemental Methods section provides all technical details.

## RESULTS

### **Silk film surface topography and stiffness direct human megakaryocyte behavior**

Porous silk films were fabricated by casting a silk solution onto a PDMS mold with different pattern (Figure 1A and Table 1). We obtained 2-5  $\mu\text{m}$  thick silk films with pores that transcended through the thickness of the films (Figure 1B). As shown in Figure 1C, surface topography significantly affected Mk adhesion as compared to non-patterned silk films. Indeed, Pattern I displayed the major improvement on Mk adhesion, while no significant differences in proplatelet formation were observed (Figure 1D). Therefore, Pattern I, was chosen as processing conditions for further characterization. Next, we reproduced different stiffness<sup>20-22</sup> (hereinafter referred as to “Low”, “Medium” and “High” protocols) in our system by varying the processing protocols and the elastic modulus was measured via AFM nano-indentation (Figure 1E). As shown in Figure 1F silk film stiffness did not significantly affect Mk adhesion, but did affect the percent of Mks that extended proplatelets, with the Low and Medium stiffness supporting significantly higher percentage of long, branched proplatelets compared to the High stiffness sample (Figures 1G and 1H). On this basis, medium stiffness was chosen as the optimum condition to maximize Mk function for further characterization.

### **Silk film ECM component functionalization supports human megakaryocyte development**

Silk films were functionalized by surface coating or entrapment with either type collagen I or fibrinogen.<sup>23-26</sup> Regardless of the functionalization method, silk films sustained similar Mk adhesion and proplatelet formation as compared to glass coverslips coated with the same molecules (Figures 2A and 2B). Further, Mk morphology was comparable in all the conditions (Figure 2C). Most importantly, Mks sensed the ECM component entrapped in the silk film. Specifically, sustained spreading and inhibition of proplatelet formation was observed on type I collagen entrapped silk films, while proplatelet formation was observed on fibrinogen entrapped films. Silk films were also functionalized with fibronectin, type IV collagen and laminin, that are the most represented ECM components around the bone marrow sinusoids.<sup>27</sup> Functionalization significantly improved both Mk adhesion and proplatelet formation over the silk film only (Figures 2D-F). Overall these data indicated that ECM components are stable inside silk films and maintain their biological activity on Mk function.

### **Co-culture with endothelial cells increases proplatelet formation and platelet release**

Silk films were mounted on plastic transwells. Endothelial primary cells (EPC) from human cord blood<sup>28</sup> were cultured on the bottom side of the silk films until confluence, and Mks seeded on the upper side (Figure 3A). Immunofluorescence imaging showed similar endothelial cell cobble-stone morphology on the silk films compared to the glass (Figures 3Bi and 3Bii) and that co-cultures

supported both Mk adhesion (Figure 3Biii) and proplatelet formation (Figure 3Biv). Importantly, Mks and endothelial cells remained localized to their respective side, separated by the functionalized porous silk film representing the discontinuous physiologic basement membrane of bone vasculature (Figures 3Bv and 3Bvi). EPCs significantly improved Mk adhesion and proplatelet formation with respect to functionalized silk only (Figure 3C). Moreover, a similar increase of both adhesion and proplatelet formation were observed by silk functionalization with human recombinant endothelial-specific molecules such as VEGF, known to enhance platelet production by CXCR4-dependent translocation of Mks to the vascular niche,<sup>29,30</sup> and VCAM-1, which interacts with the very late antigen-4 mediating Mk attachment and localization to vascular niche (Figure 3C).<sup>13,31</sup> Platelet gate and CD61/CD42b fluorescence were set upon peripheral blood platelet analysis (Figure 3D).<sup>32-34</sup> Interestingly, Mk/EPCs co-culture and VEGF/VCAM-1 inclusion determined a 4-fold and 3-fold increase, respectively, in platelet production with respect to silk films functionalized with ECM components only (Figure 3E).

### **Silk tube mimics bone marrow microvasculature and allows platelet flow**

In order to mimic bone marrow microvasculature, we fabricated microtubes<sup>19</sup> functionalized via entrapment of ECM components and SDF-1 $\alpha$  as chemo-attractant. The resulting porous silk microtubes, that exhibited physiologically relevant wall thickness ( $50\pm 20$   $\mu\text{m}$ ) (Figure 4A), were fitted into a bioreactor chamber. Interestingly, functionalized microtubes supported significantly higher Mk adhesion with respect to non-functionalized silk microtubes (Supplemental Figure 1). The biocompatible and non-thrombogenic properties of microtubes were demonstrated by perfusion of whole peripheral blood or isolated peripheral blood platelets into the silk microtubes at physiologic shear rate of  $60\text{ s}^{-1}$  (Figure 4B).<sup>35,36</sup> As shown in Figure 4C complete blood counts, before and after perfusion, were almost comparable. Moreover, upon the passage through the functionalized microtubes, platelets remained quiescent and maintained their capability of responding to physiological stimuli from adenosine diphosphate (ADP) or thrombin (Figure 4D). No signs of clot formation were observed (Figure 4E).

### **A silk sponge mimics the 3D structure of the bone marrow environment and supports platelet formation**

To mimic the 3D spongy architecture that surrounds the marrow vasculature, we assembled a silk sponge around the functionalized silk microtubes and analyzed its properties in supporting Mk function (Figure 5A). Scanning electron microscopy and immunofluorescence confocal microscopy showed that silk sponge consisted of interconnected pores approximately  $100\text{-}500$   $\mu\text{m}$  in diameter (Figures 5B and 5Ci). A total of  $2.5\times 10^5$  mature cord blood-derived Mks were seeded into the system. Human CD61<sup>+</sup> Mks not extending proplatelets could be observed 30 minutes after seeding as round and homogeneously distributed cells in the scaffold (Figure 5Cii). Longer incubation revealed changes in Mk localization and morphology. Specifically, after 16 hours Mks migrated

toward the vascular tube and adhered to the outer wall (Figure 5Ciii). Furthermore, proplatelet forming Mks distributed along the external wall of the microtubes (Figure 5Civ) and platelet tips protruding into the microtube lumen could be identified (Figure 5Cv). Finally, after 24 hours whole branched proplatelets were extended into the lumen in order to release platelets (Figure 5Cvi). Similar morphological changes were further observed by SEM imaging of parallel samples (Figures 5Di-vi). Interestingly, in the absence of SDF-1 $\alpha$  fewer Mks reached the microtube surface, with proplatelet formation occurring mainly within sponge pores, thus underlying the role of the chemo-attractant in regulating Mk migration (Supplemental Figures 2A and 2B).

### **Human megakaryocytes release functional platelets into the perfused vascular silk tube lumen**

Blood flow was mimicked by perfusing culture media into the silk microtube at a shear rate of  $60 \text{ s}^{-1}$ . The flow through of the vascular microtube was collected into a gas-permeable collection bag containing acid citrate dextrose (ACD) as anticoagulant (Figure 6A). Collected platelets were double stained with anti-CD61 and anti-CD42b antibodies and exhibited similar physical parameters as human peripheral blood platelets, as determined by flow cytometry analysis (Figure 6A). The mean number of CD61<sup>+</sup>CD42b<sup>+</sup> collected platelets was  $1.4 \pm 0.6 \times 10^6$  per 3D tissue perfusion system and linearly increased with the use of multiple bioreactors in parallel (Figure 6A). Moreover, perfusion with erythrocytes suspended in culture medium at 5% of hematocrit did not enhance platelet production as compared to media only (Supplemental Figure 3). *Ex vivo* produced platelets morphology, characterized by light microscopy and  $\beta$ 1-tubulin immunofluorescence staining, showed all the typical stages of platelet shedding: large cytoplasmic fragments resembling pre-platelets intermediates ( $>4 \mu\text{m}$  diameter), dumbbell-shaped platelets, and standard disc-shaped platelet ( $2\text{-}4 \mu\text{m}$  diameter) (Figures 6Bi-v).  $\beta$ 1-tubulin was mainly distributed at platelet perimeter into the typical platelet microtubule coil (Figures 6Biv and 6Bv). Platelets ultra-structure, imaged by transmission electron microscopy (TEM), showed the presence of physiological alpha- and dense-granules (Figure 6Bvi). Parallel flow cytometry analysis of collected platelets, in presence of calcein-AM, gave demonstration that almost all analyzed particles were live cells. Importantly, collected platelets kept in transfusional bags, at room temperature with constant agitation, were still alive up to 4 days from collection (data not shown).

### ***Ex vivo* produced platelets are functional and can contribute to clot formation**

We proceeded to analyze the functionality of *ex vivo* produced platelets. Actin staining demonstrated no relevant cytoskeleton organization in resting platelets (Figure 6Ci), while, after seeding onto immobilized type I collagen, platelets spread by assembling actin stress fibers (Figures 6Cii-iv). In order to test platelet functionality in a condition closely mimicking vessel injury we took advantage of a well characterized flow chamber system, widely employed to study platelet functions.<sup>37,38</sup> For this experiment, Mks were stained with  $0.5 \mu\text{M}$  carboxyfluorescein diacetate

succinimidyl ester (CFSE) cell staining dye, before being seeded into the silk-based system. CFSE<sup>+</sup> produced platelets were resuspended, to a final concentration of 4X10<sup>6</sup>/mL, in Tyrode's buffer containing 100 µg/mL von Willebrand Factor and perfused over immobilized type I collagen at a shear rate of 1000 s<sup>-1</sup>.<sup>39</sup> We observed platelet arrest and adhesion onto the substrate with formation of small platelet aggregates, thus suggesting their ability to promote thrombus formation (Figure 6Cv). This function was further confirmed by a flow cytometry-based platelet aggregation assay,<sup>40</sup> in which collected platelets were split and single stained with two different antibodies, anti-CD31 and anti-CD42b. Upon union of both platelets populations and activation, we observed the appearance of a double-colored population of aggregated platelets compared to the unactivated control (Figure 6D). Platelet function was finally assessed by the study of *ex vivo* produced platelets participation to clot formation *in vitro*.<sup>41,42</sup> CFSE<sup>+</sup> platelets from our tissue system were mixed with peripheral blood platelet stained with CellTracker Deep Red Dye in Tyrode's buffer containing 1 mg/mL fibrinogen and 1 U/mL thrombin. As shown in Figure 6Ei CFSE<sup>+</sup> platelets were distributed homogeneously within the sample. Importantly, peripheral blood (red) and *ex vivo* produced platelets (green) were shown to actively interact based on the appearance of overlapping staining (yellow), thus demonstrating the contribution of the latter to clot formation (Figure 6Eii).

#### **Silk vascular tubes can be coated with a confluent endothelium or functionalized with endothelial cells-derived molecules**

To further mimic the composition of the vascular niche, HMVEC-d or EPCs were cultured within the silk microtube lumen prior to seeding Mks into the silk sponge (Figure 7A).<sup>43,44</sup> Endothelial cells formed a confluent layer covering the inner wall of the silk microtubes with the characteristic cobblestone morphology and VE-cadherin staining (Figures 7Bi and 7Bii). Endothelialized vascular microtubes exhibited a significant increase in the number of collected platelets compared to non-endothelialized silk vascular microtubes (Figure 7C). No differences were observed between the two endothelial cell sources (data not shown). Interestingly, silk functionalization with VEGF and VCAM-1, recapitulated the increase in platelet production observed in the presence of endothelium (Figure 7C).

Platelet functionality was determined by flow cytometry analysis of increased PAC-1 binding to the activated integrin  $\alpha_{IIb}\beta_3$ , upon physiologic stimulation with both weak (i.e. epinephrine, ADP) and strong (i.e. thrombin) agonists, with respect to resting conditions (Supplemental Figure 4A). No differences were observed between presence or absence of endothelial cells (Supplemental Figure 4B).

#### **Analysis of *ex vivo* platelet production from human megakaryocytes derived from adult hematopoietic progenitor cells**

We finally investigated how Mks derived from peripheral blood progenitors of healthy subjects and patients with primary myelofibrosis behaved within the system. Time course analysis revealed



similar Mk behavior to that observed with cord-blood derived Mks, with CD61<sup>+</sup> round Mks homogeneously distributed within the sponge at the beginning of the experiment and proplatelet extension across the tube lumen after 24 hours incubation (Figures 8Ai-vi). However, patient 1 derived Mks displayed higher branched proplatelets, while patient 2 fewer and shorter proplatelet shafts, than healthy control (Figures 8Aiv-vi). This evidence was paralleled by an increase in CD61<sup>+</sup>CD42b<sup>+</sup> platelets release by patient 1 Mks and a reduced number of collected platelets from patient 2 with respect to healthy control (Figure 8B). Results obtained were further supported by the comparison of *ex vivo* and *in vivo* platelet count (Figure 8C). Interestingly, patient 1, who showed the higher thrombopoietic potential in our 3D system, had an history of high peripheral blood platelet count, while patient 2, characterized by a reduced *ex vivo* platelet biogenesis, presented a low platelet count compared to physiologic range. These data are consistent with our previous finding demonstrating a significant correlation between *in vivo* platelet count and *in vitro* proplatelet formation from patients with myeloproliferative neoplasms.<sup>45</sup>

## DISCUSSION

Silk protein can be transformed into a wide range of material formats that can be integrated to reproduce a niche-like bone marrow microenvironment. Through a complete redesign of our initial model,<sup>2</sup> we engineered a 3D bone marrow model made of porous silk to fully recreate the physiology of human bone marrow niche environment. Our new system is capable of successfully generating functional platelets *ex vivo*, with endothelial cells co-cultures significantly increasing the numbers of released platelets.

Thanks to this novel system we identified and exploited numerous unique properties of silk biomaterial for physiologically relevant bone marrow modeling and platelet production. First, we modelled silk to control topography and stiffness, both features that have been shown to affect Mk adhesion and proplatelet formation.<sup>21,46</sup> Cells *in vivo* are exposed to diverse topographies, depending on tissue structure and ECM composition that may exert a major impact on their function.<sup>47-49</sup> We demonstrated that lower surface roughness results in a better outcome in terms of Mk adhesion, consistent with the notion that perivascular space is mainly a continuous surface.<sup>22</sup> In contrast, Mk adhesion was unaffected by substrate stiffness whereas proplatelet formation and branching decreased on stiffer substrates. The rigidity of the human basement membrane located in the perivascular space is still unclear.<sup>22</sup> However, these results are consistent with the evidence that soft substrates better sustain platelet production.<sup>21</sup> Second, we functionalized the silk by either surface coating or entrapment of ECM components. The advantage of entrapping the ECM components within the silk film is that silk has been shown to stabilize bioactive molecules at physiologic conditions without loss of bioactivity.<sup>50</sup> Accordingly, there was no difference between Mk adhesion and proplatelet formation on functionalized silk films that had been coated or that had the ECM protein entrapped within the film as Mks were able to sense the ECM component entrapped in the silk film and behave consequently. Then, we cultured endothelial cells with Mks



under experimental settings where the two cell types were physically separated by functionalized silk. Mks/endothelial cells co-culture has shown that chemokines released by the endothelial cells contribute to Mk maturation, Mk localization to the vascular niche, and increased platelet production.<sup>13</sup> Additionally, Mk adhesion to endothelial cells increases Mk proliferation and maturation.<sup>12,31,51</sup> We confirmed the importance of Mks and endothelial cells co-culture by measuring a significant increase in platelet production in the co-culture conditions compared to the Mk-only cultures, suggesting that the tunable features of the silk film model, namely ECM entrapment, surface topography, and stiffness, optimized with the concomitant presence of endothelial cells can support platelet production and release *ex vivo*. In addition, we observed that silk functionalization with VEGF and VCAM-1, recapitulated the increase in platelet production observed in the presence of endothelium, thus suggesting that endothelial cells could be replaced by recombinant endothelial derived molecules.

The insights gained with the basement membrane model guided us in the assembly of the silk-sponge based bone marrow system closely mimicking the 3D bone marrow structure and composition with great improvement with respect to our previous model.<sup>2</sup> Specifically, a silk sponge mimicked the 3D environment where hematopoiesis takes place; while entrapment of ECM components and SDF-1 $\alpha$  in silk microtube wall allowed us to avoid the use of gels, thus obtaining a chemo-attractive thin basement membrane-like layer of silk. Finally, blood flow was mimicked by perfusion of culture media at a shear rate of 60 s<sup>-1</sup> that has been described to be exerted into mouse bone marrow sinusoids and to promote platelet production by human Mks.<sup>35,36</sup> Importantly, media perfusion improved the yield of released platelets through the 3D silk tissue with respect to static condition, while perfusion with reconstituted red blood cells did not impact on platelet production. However, the perfusion of red blood cells represents an important step to strengthen our strategy in reproducing the physiological blood flow of the vascular bone marrow niche and in future will offer the unique possibility to modulate oxygen tension inside the system.<sup>52,53</sup> Interestingly, further increase in the number of collected platelets was obtained by the presence of endothelial cells within the tube lumen or silk functionalization with endothelium derived recombinant molecules, thus indicating that for future scaled-up production we will be able to avoid the use of endothelial cells by mixing silk with these or others specific recombinant molecules of endothelial origin able to promote Mk function.

Overall, the combination of the unique features of the present model together with the modular bioreactor setup led to a 3-fold increase in total platelet yield as compared to our previous system.<sup>2</sup> Thus, the more closely we mimic the bone marrow environment the greater number of platelets are collected. Even though the number of platelets per Mk may be considered still low with respect to estimated values *in vivo*,<sup>54</sup> making this a major point to be investigated, we believe that being able to produce sufficient platelets suitable for further analysis is a fundamental advantage toward understanding the mechanisms of platelet production in healthy and disease conditions. To this regard, the improvements of this new system allowed us to better characterize *ex vivo* produced

platelet morphology by different microscopy approaches and platelet functionality by a variety of *in vitro* assays demonstrating the ability to aggregate and form thrombi. Most importantly, we demonstrated that similar platelet production can be obtained by exploiting our system with hematopoietic progenitor cells from different sources, including patient derived Mks. Interestingly, a significant correlation among proplatelet branching along the silk vascular tube, the extent of platelet release *ex vivo* and *in vivo* platelet count was observed when Mks, derived from patients with primary myelofibrosis,<sup>45</sup> were seeded in the bone marrow model. This in turn leads us to believe that our system will provide unique opportunities for clinical applications.

Different 3D tools have been described so far in the attempt of supporting thrombopoiesis by both mouse and human Mks differentiated from either hematopoietic progenitors or the promising induced pluripotent stem cells.<sup>4,5,55-59</sup> Despite the usefulness for the advancement in providing systems for platelet production, all these models did not reproduce the complex microenvironment where megakaryopoiesis physiologically takes place. In this regard, a fundamental advantage of our model is its ability to provide the first *ex vivo* tissue system able to reproduce the 3D structure of the bone marrow niche, in combination with ECM components and physiologic shear rate, for the study of Mk function and platelet formation. Going forward with this system should provide a platform for studying mechanisms of megakaryopoiesis for further elucidation of the processes that regulate platelet production. This insight will in turn shed light on megakaryopoiesis related disease progression. Patient-derived Mks and endothelial cells, which can be derived from several depots throughout the body, can be cultured in this model and used to design patient-specific drug administration regimes. Additionally, *ex vivo* generated platelets could be used as a source of growth factors for wound healing in regenerative medicine, including healing of recalcitrant ulcers and burns, and stimulation of osseous tissue regeneration in dentistry and maxillofacial plastic surgery.<sup>60</sup> Lastly, this 3D bone marrow tissue perfusion system provides a versatile tool for studying hematopoiesis *ex vivo* offering additional opportunities in elucidating fundamental biological mechanisms of hematopoiesis and for clinical application in diagnosing and treating disease while avoiding the need for animal models.

## ACKNOWLEDGEMENTS

We thank Centro Grandi Strumenti of the University of Pavia, Dr. Patrizia Vaghi and Dr. Vittorio Necchi for technical assistance with confocal and transmission electron microscopy; Dr. Gianluca Viarengo, Dr. Laura Vanelli and Prof. Federica Meloni for technical assistance with the flow cytometry analysis; Dr. Cesare Perotti and Dr. Laura Salvaneschi for supplying human cord and peripheral blood; Dr. Mario Mazzucato and Dr. Monica Battiston for technical assistance in the study of platelet adhesion under flow; Dr. Giovanni Barosi and Dr. Vittorio Rosti for supplying patients' peripheral blood; Prof. Joseph Italiano for providing  $\beta$ 1-tubulin antibody. This paper was supported by Cariplo Foundation (2010-0807), US National Institutes of Health (grant EB016041-01), Italian Ministry of Health (grant RF-2009-1550218 and RF-2010-2316198) and Italian Ministry

of University and Research, FIRB (RBFR1299KO). The funders had no role in study design, data collection and analysis, decision to publish, or preparation of the manuscript.

### **AUTHORSHIP CONTRIBUTIONS**

A.B. conceived the idea, supervised the project and wrote the manuscript; C.A.D.B., L.S.W., L.T. and A.M. designed and performed the experiments, analyzed the data and wrote the manuscript; Y.C., C.E.G., D.S., C.S., A.A., E.S. and G.B. performed the experiments and edited the manuscript; C.S., L.D.M., M.M., and D.L.K. analyzed the data and edited the manuscript.

### **DISCLOSURE OF CONFLICTS OF INTEREST**

The authors declare no competing financial interests.

### **REFERENCES**

1. DeZern AE, Sekeres MA. The Challenging World of Cytopenias: Distinguishing Myelodysplastic Syndromes From Other Disorders of Marrow Failure. *Oncologist*. 2014;19(7):735-745.
2. Pallotta I, Lovett M, Kaplan DL, Balduini A. Three-dimensional system for the in vitro study of megakaryocytes and functional platelet production using silk-based vascular tubes. *Tissue Eng Part C Methods*. 2011;17(12):1223-1232.
3. Torisawa YS, Spina CS, Mammoto T, et al. Bone marrow-on-a-chip replicates hematopoietic niche physiology in vitro. *Nat Methods*. 2014;11(6):663-669.
4. Nakagawa Y, Nakamura S, Nakajima M, et al. Two differential flows in a bioreactor promoted platelet generation from human pluripotent stem cell-derived megakaryocytes. *Exp Hematol*. 2013;41(8):742-748.
5. Thon JN, Mazutis L, Wu S, et al. Platelet bioreactor-on-a-chip. *Blood*. 2014.
6. Morrison SJ, Scadden DT. The bone marrow niche for haematopoietic stem cells. *Nature*. 2014;505(7483):327-334.
7. Wang LD, Wagers AJ. Dynamic niches in the origination and differentiation of haematopoietic stem cells. *Nat Rev Mol Cell Biol*. 2011;12(10):643-655.
8. Inoue S, Osmond DG. Basement membrane of mouse bone marrow sinusoids shows distinctive structure and proteoglycan composition: a high resolution ultrastructural study. *Anat Rec*. 2001;264(3):294-304.
9. Ohta M, Sakai T, Saga Y, Aizawa S, Saito M. Suppression of hematopoietic activity in tenascin-C-deficient mice. *Blood*. 1998;91(11):4074-4083.
10. Jacenko O, Roberts DW, Campbell MR, McManus PM, Gress CJ, Tao Z. Linking hematopoiesis to endochondral skeletogenesis through analysis of mice transgenic for collagen X. *Am J Pathol*. 2002;160(6):2019-2034.

11. Winkler IG, Barbier V, Nowlan B, et al. Vascular niche E-selectin regulates hematopoietic stem cell dormancy, self renewal and chemoresistance. *Nat Med*. 2012;18(11):1651-1657.
12. Rafii S, Shapiro F, Pettengell R, et al. Human bone marrow microvascular endothelial cells support long-term proliferation and differentiation of myeloid and megakaryocytic progenitors. *Blood*. 1995;86(9):3353-3363.
13. Avecilla ST, Hattori K, Heissig B, et al. Chemokine-mediated interaction of hematopoietic progenitors with the bone marrow vascular niche is required for thrombopoiesis. *Nat Med*. 2004;10(1):64-71.
14. Junt T, Schulze H, Chen Z, et al. Dynamic visualization of thrombopoiesis within bone marrow. *Science*. 2007;317(5845):1767-1770.
15. Vepari C, Kaplan DL. Silk as a Biomaterial. *Prog Polym Sci*. 2007;32(8-9):991-1007.
16. Lovett M, Cannizzaro C, Daheron L, Messmer B, Vunjak-Novakovic G, Kaplan DL. Silk fibroin microtubes for blood vessel engineering. *Biomaterials*. 2007;28(35):5271-5279.
17. Lawrence BD, Marchant JK, Pindrus MA, Omenetto FG, Kaplan DL. Silk film biomaterials for cornea tissue engineering. *Biomaterials*. 2009;30(7):1299-1308.
18. Rockwood DN, Preda RC, Yücel T, Wang X, Lovett ML, Kaplan DL. Materials fabrication from Bombyx mori silk fibroin. *Nat Protoc*. 2011;6(10):1612-1631.
19. Lovett ML, Cannizzaro CM, Vunjak-Novakovic G, Kaplan DL. Gel spinning of silk tubes for tissue engineering. *Biomaterials*. 2008;29(35):4650-4657.
20. Cox TR, Ertler JT. Remodeling and homeostasis of the extracellular matrix: implications for fibrotic diseases and cancer. *Dis Model Mech*. 2011;4(2):165-178.
21. Malara A, Gruppi C, Pallotta I, et al. Extracellular matrix structure and nano-mechanics determine megakaryocyte function. *Blood*. 2011;118(16):4449-4453.
22. Charras G, Sahai E. Physical influences of the extracellular environment on cell migration. *Nat Rev Mol Cell Biol*. 2014;15(12):813-824.
23. Balduini A, Pallotta I, Malara A, et al. Adhesive receptors, extracellular proteins and myosin IIA orchestrate proplatelet formation by human megakaryocytes. *J Thromb Haemost*. 2008;6(11):1900-1907.
24. Malara A, Gruppi C, Rebuzzini P, et al. Megakaryocyte-matrix interaction within bone marrow: new roles for fibronectin and factor XIII-A. *Blood*. 2011;117(8):2476-2483.
25. Lu Q, Wang X, Hu X, Cebe P, Omenetto F, Kaplan DL. Stabilization and release of enzymes from silk films. *Macromol Biosci*. 2010;10(4):359-368.
26. Gil ES, Panilaitis B, Bellas E, Kaplan DL. Functionalized silk biomaterials for wound healing. *Adv Healthc Mater*. 2013;2(1):206-217.
27. Malara A, Currao M, Gruppi C, et al. Megakaryocytes contribute to the bone marrow-matrix environment by expressing fibronectin, type IV collagen, and laminin. *Stem Cells*. 2014;32(4):926-937.

28. Ingram DA, Mead LE, Tanaka H, et al. Identification of a novel hierarchy of endothelial progenitor cells using human peripheral and umbilical cord blood. *Blood*. 2004;104(9):2752-2760.
29. Thiele W, Krishnan J, Rothley M, et al. VEGFR-3 is expressed on megakaryocyte precursors in the murine bone marrow and plays a regulatory role in megakaryopoiesis. *Blood*. 2012;120(9):1899-1907.
30. Pitchford SC, Lodie T, Rankin SM. VEGFR1 stimulates a CXCR4-dependent translocation of megakaryocytes to the vascular niche, enhancing platelet production in mice. *Blood*. 2012;120(14):2787-2795.
31. Avraham H, Cowley S, Chi SY, Jiang S, Gropman JE. Characterization of adhesive interactions between human endothelial cells and megakaryocytes. *J Clin Invest*. 1993;91(6):2378-2384.
32. Cramer EM, Norol F, Guichard J, et al. Ultrastructure of platelet formation by human megakaryocytes cultured with the Mpl ligand. *Blood*. 1997;89(7):2336-2346.
33. Takayama N, Nishikii H, Usui J, et al. Generation of functional platelets from human embryonic stem cells in vitro via ES-sacs, VEGF-promoted structures that concentrate hematopoietic progenitors. *Blood*. 2008;111(11):5298-5306.
34. Nakamura S, Takayama N, Hirata S, et al. Expandable megakaryocyte cell lines enable clinically applicable generation of platelets from human induced pluripotent stem cells. *Cell Stem Cell*. 2014;14(4):535-548.
35. Mazo IB, von Andrian UH. Adhesion and homing of blood-borne cells in bone marrow microvessels. *J Leukoc Biol*. 1999;66(1):25-32.
36. Jiang J, Woulfe DS, Papoutsakis ET. Shear enhances thrombopoiesis and formation of microparticles that induce megakaryocytic differentiation of stem cells. *Blood*. 2014;124(13):2094-2103.
37. Mazzucato M, Cozzi MR, Battiston M, et al. Distinct spatio-temporal Ca<sup>2+</sup> signaling elicited by integrin alpha2beta1 and glycoprotein VI under flow. *Blood*. 2009;114(13):2793-2801.
38. Mazzucato M, Cozzi MR, Pradella P, Ruggeri ZM, De Marco L. Distinct roles of ADP receptors in von Willebrand factor-mediated platelet signaling and activation under high flow. *Blood*. 2004;104(10):3221-3227.
39. Ruggeri ZM, Mendolicchio GL. Adhesion mechanisms in platelet function. *Circ Res*. 2007;100(12):1673-1685.
40. De Cuyper IM, Meinders M, van de Vijver E, et al. A novel flow cytometry-based platelet aggregation assay. *Blood*. 2013;121(10):e70-80.
41. Tuszyński GP, Kordecki E, Cierniewski C, et al. Association of fibrin with the platelet cytoskeleton. *J Biol Chem*. 1984;259(8):5247-5254.
42. Rooney MM, Parise LV, Lord ST. Dissecting clot retraction and platelet aggregation. Clot retraction does not require an intact fibrinogen gamma chain C terminus. *J Biol Chem*. 1996;271(15):8553-8555.

43. Borges J, Mueller MC, Padron NT, Tegtmeier F, Lang EM, Stark GB. Engineered adipose tissue supplied by functional microvessels. *Tissue Eng.* 2003;9(6):1263-1270.
44. Wenger A, Stahl A, Weber H, et al. Modulation of in vitro angiogenesis in a three-dimensional spheroidal coculture model for bone tissue engineering. *Tissue Eng.* 2004;10(9-10):1536-1547.
45. Balduini A, Badalucco S, Pugliano MT, et al. In vitro megakaryocyte differentiation and proplatelet formation in Ph-negative classical myeloproliferative neoplasms: distinct patterns in the different clinical phenotypes. *PLoS One.* 2011;6(6):e21015.
46. Shin JW, Swift J, Spinler KR, Discher DE. Myosin-II inhibition and soft 2D matrix maximize multinucleation and cellular projections typical of platelet-producing megakaryocytes. *Proc Natl Acad Sci U S A.* 2011;108(28):11458-11463.
47. Feng Q, Chai C, Jiang XS, Leong KW, Mao HQ. Expansion of engrafting human hematopoietic stem/progenitor cells in three-dimensional scaffolds with surface-immobilized fibronectin. *J Biomed Mater Res A.* 2006;78(4):781-791.
48. Dellatore SM, Garcia AS, Miller WM. Mimicking stem cell niches to increase stem cell expansion. *Curr Opin Biotechnol.* 2008;19(5):534-540.
49. Kim DH, Provenzano PP, Smith CL, Levchenko A. Matrix nanotopography as a regulator of cell function. *J Cell Biol.* 2012;197(3):351-360.
50. Zhang J, Pritchard E, Hu X, et al. Stabilization of vaccines and antibiotics in silk and eliminating the cold chain. *Proc Natl Acad Sci U S A.* 2012;109(30):11981-11986.
51. Hamada T, Möhle R, Hesselgesser J, et al. Transendothelial migration of megakaryocytes in response to stromal cell-derived factor 1 (SDF-1) enhances platelet formation. *J Exp Med.* 1998;188(3):539-548.
52. Magnani M, Rossi L, Bianchi M, et al. Improved stability of 2,3-bisphosphoglycerate during storage of hexokinase-overloaded erythrocytes. *Biotechnol Appl Biochem.* 1989;11(5):439-444.
53. Cabrales P, Tsai AG, Intaglietta M. Modulation of perfusion and oxygenation by red blood cell oxygen affinity during acute anemia. *Am J Respir Cell Mol Biol.* 2008;38(3):354-361.
54. Kaufman RM, Airo R, Pollack S, Crosby WH. Circulating megakaryocytes and platelet release in the lung. *Blood.* 1965;26(6):720-731.
55. Sullenbarger B, Bahng JH, Gruner R, Kotov N, Lasky LC. Prolonged continuous in vitro human platelet production using three-dimensional scaffolds. *Exp Hematol.* 2009;37(1):101-110.
56. Lasky LC, Sullenbarger B. Manipulation of oxygenation and flow-induced shear stress can increase the in vitro yield of platelets from cord blood. *Tissue Eng Part C Methods.* 2011;17(11):1081-1088.
57. Schlinker AC, Radwanski K, Wegener C, Min K, Miller WM. Separation of in-vitro-derived megakaryocytes and platelets using spinning-membrane filtration. *Biotechnol Bioeng.* 2014.
58. Feng Q, Shabrani N, Thon JN, et al. Scalable generation of universal platelets from human induced pluripotent stem cells. *Stem Cell Reports.* 2014;3(5):817-831.



59. Lambert MP, Sullivan SK, Fuentes R, French DL, Poncz M. Challenges and promises for the development of donor-independent platelet transfusions. *Blood*. 2013;121(17):3319-3324.

60. Anitua E, Andia I, Ardanza B, Nurden P, Nurden AT. Autologous platelets as a source of proteins for healing and tissue regeneration. *Thromb Haemost*. 2004;91(1):4-15.

## TABLE

**Table 1. Spatial parameters of the surface patterns used.**

Pattern	Depth (nm±SD)	Width (nm±SD)	Roughness (nm±SD)
None	--	--	3.2±0.5
I	39±5.3	445±33	11.6±1.6
II	64±4.1	1796±173	19.5±1.3
III	465±55	1898±113	156.7±13.8

## FIGURE LEGENDS

**Figure 1. Effect of silk film topography and stiffness on human megakaryocyte adhesion and proplatelet formation.** (A) Silk films are prepared by dispensing a silk and polyethylene oxide (PEO) solution onto a polydimethylsiloxane (PDMS) mold. The surface of the mold may contain a grating pattern with defined depth and width. When the solution dries, a silk film is formed that contains a dispersion of PEO porogen. The film is finally soaked in PBS to remove the PEO porogen. (B) Representative light microscopy image of silk film porosity (scale bar=25  $\mu$ m). (C, D) Analysis of Mk adhesion and proplatelet formation on silk film with different topography coated with fibrinogen (average±SD, n=3, \*p<0.05). Results are presented relative to silk film with no pattern. (E) AFM elastic modulus values obtained over hydrated Low, Medium, and High films. Distributions are displayed as percent of total sample points measured per bin. All samples had a minimum of 300 measurements. (F) There was no significant difference in Mk adhesion between the different stiffness samples (average±SD, n=4, p=NS). (G) The low stiffness samples had similar proplatelet formation compared to the medium stiffness, but significantly higher percentage compared to the high stiffness samples (average±SD, n=4, \*p<0.01). (H) Representative  $\beta$ 1-tubulin staining of Mks cultured on silk films with different stiffness coated with fibrinogen, after 16 hours incubation. The low stiffness silk films supported long proplatelet extensions and increased silk film stiffness appeared to decreased proplatelet branching (scale bar=50  $\mu$ m).

**Figure 2. Effect of silk film functionalization on human megakaryocyte adhesion and proplatelet formation.** (A, B) Mk adhesion and proplatelet formation on ECM entrapped within silk film followed a similar trend compared to ECM coated on glass coverslip or coated on silk film (average±SD, n=4, p=NS). (C) Representative  $\alpha$ -tubulin staining of Mks cultured on coated glass coverslip, coated silk film or entrapped silk film. Mks were able to sense the proteins entrapped in silk film as they normally spread on type I collagen and form proplatelet on fibrinogen in all tested



conditions (scale bar=50  $\mu\text{m}$ ). (D, E) Analysis of silk film functionalization with bone marrow vascular niche ECM components: fibronectin (FNC), type IV collagen (COL IV), laminin (LAM). Both Mk adhesion and proplatelet formation were not different between the three tested ECM components, but significantly higher compared to the non-functionalized silk film control only (average $\pm$ SD, n=3, \*p<0.05). (F) Representative  $\beta$ 1-tubulin staining of Mks cultured for 16 hours on functionalized silk films shows that proplatelet morphology was almost similar between the three tested conditions (scale bar=50  $\mu\text{m}$ ).

**Figure 3. Role of endothelial cells and endothelial-derived molecules in the regulation of platelet formation within the silk film culture system.** (A) Schematic of the EPC and Mk seeding procedure for establishment of the silk film model. (B) After 16 hours of culture on the basal side of the silk film membrane, EPCs exhibited the characteristic cobblestone morphology and expression of VE-cadherin on both glass coverslip control (Bi) and functionalized silk film (Bii) (green= VE-cadherin, blue=nuclei, scale bar=100  $\mu\text{m}$ ). (Biii, Biv) Representative fluorescent image of Mk and EPC co-culture on the silk film culture system (green=VE-Cadherin, red=CD61, blue=nuclei, scale bar= 50  $\mu\text{m}$ ). (Bv, Bvi) Representative cross-section image of Mk and EPC co-culture rendered using confocal microscopy. There was distinct localization of the EPCs (green) on the basal side of the membrane and Mks (red) on the upper side of the membrane (green=VE-Cadherin, red=CD61, blue=nuclear, scale bar=20  $\mu\text{m}$ ). Silk films were stained with Hoechst 33258 and visualized in blue. (C) Analysis of Mk adhesion and proplatelet formation on silk film functionalized with ECM components in the presence or not of EPCs or VEGF and VCAM-1 (average $\pm$ SD, n=6, \*p<0.05). (D) CD61<sup>+</sup>CD42b<sup>+</sup> peripheral blood platelets were used to set the platelet gating protocol. Samples were mixed with counting beads in order to quantify the number of released platelets. Average $\pm$ SD of the mean fluorescence intensity (MFI) of CD61 and CD42b staining from 6 different experiments is reported (p=NS). (E) Mks cultured on functionalized silk film in the presence of EPCs or VEGF and VCAM-1 produced a significantly increased number of platelets compared to functionalized silk film only (average $\pm$ SD, n=6, \*p<0.01).

**Figure 4. Silk microtube fabrication and analysis of their ability to support platelet perfusion.** (A) Silk microtubes are prepared by gel spinning aqueous silk solutions containing polyethylene oxide (PEO) porogen around a wire and functionalized via entrapment of ECM components. Resulting microtubes are freeze-dried, removed from the wire and soaked in water to leach out the PEO porogen. The resulting porous silk microtubes are fitted into the bioreactor chamber. (Ai) Scanning electron microscopy (SEM) cross sections of a silk microtube: microtube wall thickness was 50 $\pm$ 20  $\mu\text{m}$  with microtube wall pores diameter of 22 $\pm$ 4  $\mu\text{m}$  to allow proplatelet elongation (scale bar=20  $\mu\text{m}$ ). Arrows indicate silk microtubes borders. (Aii, Aiii) SEM images show pores on both the inner and outer surfaces of the silk microtubes, respectively. The inner and outer microtube wall pores diameter was 6 $\pm$ 2  $\mu\text{m}$  (scale bars=20  $\mu\text{m}$ ). (B) Whole blood (red) or

peripheral blood platelets suspended in culture medium (pink) were perfused into functionalized silk microtubes. (C) Representative analysis of whole blood cells of one sample before (inlet) or after (outlet) perfusion. WBC=white blood cells; RBC=red blood cells; HCT=hematocrit; MCV=mean corpuscular volume; MCH=mean corpuscular hemoglobin; MCHC=mean corpuscular hemoglobin concentration; RDW=red blood cell distribution width; PLT=platelet. (D) Representative flow cytometry analysis of peripheral blood platelet basal activation before and after perfusion into silk microtube. Activation with ADP and thrombin demonstrated increased PAC-1 binding indicating normal CD42b<sup>+</sup> platelet functionality after the passage through the silk microtube lumen. (E) Confocal microscopy analysis of CD61<sup>+</sup> platelet distribution within microtube lumen after passage of whole blood (green=CD61; blue=nuclei; scale bar=50  $\mu$ m).

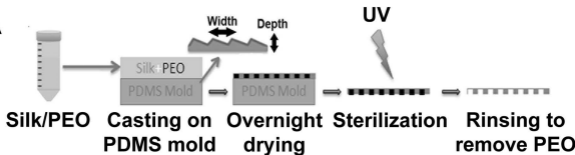
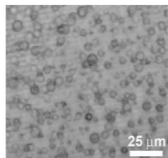
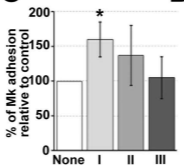
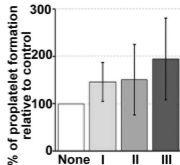
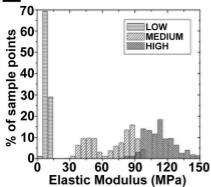
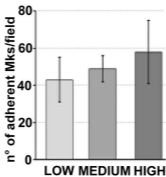
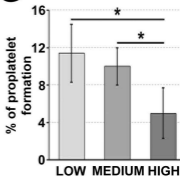
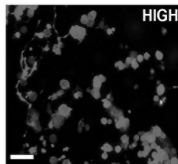
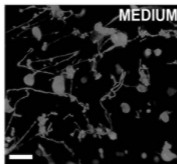
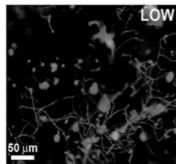
**Figure 5. Silk microtube assembly and sponge preparation into the bioreactor chamber and analysis of platelet production within this system.** (A) Aqueous silk is dispensed into the chamber around the microtube and salt particles are added. After leaching out the salt, the resulting porous silk sponge is trimmed and sterilized. After seeding into the silk sponge Mks migrate toward the microtube, adhere and extend proplatelets through the microtube wall to release platelets into the microtube lumen. (Bi) SEM image showing a silk microtube embedded into the silk sponge (scale bar=100  $\mu$ m). (Bii) SEM image showing the porous morphology of silk sponge (scale bar=100  $\mu$ m). (C) Confocal microscopy analysis of different steps of Mks behavior within the silk microtube-sponge tissue system. (Ci) Silk sponge before Mks seeding (scale bar=100  $\mu$ m). (Cii) Mature Mks immediately after seeding into the silk sponge (green=CD61; blue=nuclei; scale bar=100  $\mu$ m). (Ciii) Migrated Mks in close contact with the microtube wall (green=CD61; blue=nuclei; scale bar=50  $\mu$ m). (Civ) Mks forming proplatelet upon adhesion to the microtube wall (green=CD61; blue=nuclei; scale bar=50  $\mu$ m). (Cv) Mk extending proplatelets through the silk microtube wall. Arrow indicates proplatelet branch elongation through microtube wall with proplatelet tip protruding into the microtube lumen (green=CD61; blue=nuclei; scale bar=50  $\mu$ m). (Cvi) Boxes highlight proplatelet branches detectable along the inner wall of the silk microtube and platelets released into the microtube lumen (green=CD61; blue=nuclei; scale bar=50  $\mu$ m). For all immunofluorescence analysis silk fibroin 3D scaffolds were stained with Hoechst 33258 and visualized in blue. (D) SEM imaging of different steps of Mks behavior within the silk microtube-sponge tissue system. (Di) Mature Mks adhesion on silk microtube outer wall (scale bar=2  $\mu$ m). (Dii, Diii) Migrated Mks forming proplatelet upon adhesion to the microtube wall (scale bar=2 and 10  $\mu$ m). Arrows indicate silk pores that allow proplatelet elongation inside microtube lumen. (Div) Longitudinal section of silk microtube-sponge tissue system (scale bar=200  $\mu$ m). (Dv) Mk extending proplatelets through silk microtube wall (scale bar=10  $\mu$ m). (Dvi) Proplatelet branch stemming inside microtube lumen and released platelets (scale bar=10  $\mu$ m).

**Figure 6. Analysis of *ex vivo* produced platelets morphology and functionality.** (A) Silk microtubes are perfused with culture media for 6 hours and released platelets are collected into gas-permeable bags. Samples are mixed with counting beads in order to quantify the number of platelets which are identified as CD61<sup>+</sup>CD42b<sup>+</sup> events. A maximum of four different silk microtubes have been perfused concurrently. The graph shows the absolute number of platelets released per microtube embedded in the silk sponge containing  $2.5 \times 10^5$  Mks. (B) Analysis of platelet morphology. (Bi, Bii) Light microscopy analysis shows pre-platelets, dumbbell-shaped platelets and disc-shaped platelet (scale bar=10  $\mu$ m). (Biii) Immunofluorescence staining of  $\beta$ 1-tubulin (green) (scale bar=10  $\mu$ m). (Biv, Bv) Magnification highlights the microtubule coil typically showed by resting platelets (scale bar=5  $\mu$ m). (Bvi) TEM analysis of *ex vivo* produced platelets ultra-structure (scale bar=2  $\mu$ m). (C) Analysis of platelet adhesion on type I collagen. (Ci) TRITC-phalloidin staining of resting platelets (scale bar=5  $\mu$ m). (Cii) After adhesion on type I collagen platelets spread and formed filopodia/lamellipodia (scale bar=5  $\mu$ m). (Ciii, Civ) Magnification highlights actin cytoskeleton reorganization with evident stress fibers assembly (scale bar=5  $\mu$ m). (Cv) CFSE<sup>+</sup> platelets were suspended into Tyrode's buffer containing von Willebrand Factor and perfused over immobilized type I collagen at shear rate of  $1000 \text{ s}^{-1}$ . Image shows a representative field demonstrating platelet adhesion. Arrows indicate formation of platelet aggregates (scale bar=10  $\mu$ m). (D) Aggregation capacity was further measured by flow cytometry after stimulation with thrombin, ADP and epinephrine. Platelets were separately labeled with CD31 or CD42b (left and right top, respectively), and then mixed 1:1, before being stimulated (bottom right) or not (bottom left) with the cocktail of agonists. (E) Analysis of *ex vivo* produced platelets participation to clot formation. (Ei) *Ex vivo* produced CFSE<sup>+</sup> platelets were mixed with peripheral blood platelet stained with CellTracker Deep Red Dye. Clot formation was favored by addition of thrombin and visualized by confocal microscopy (scale bar=10  $\mu$ m). (Eii) Cross-section analysis of z-stack of the clot demonstrating that *ex vivo* produced platelets (green) actively interacted with *in vivo* derived platelets (red) with appearance of a juxtaposed signal (yellow) (scale bar=5  $\mu$ m).

**Figure 7. Adding complexity to the system: endothelial and endothelial-derived molecules promote platelet collection.** (A) The silk microtube lumen supports a confluent monolayer of human endothelial cells. (Bi) Confocal microscopy images of confluent human dermal microvascular endothelial cells (HMVEC-d) into the silk microtube lumen (green=VE-cadherin; scale bar=100  $\mu$ m). (Bii) Magnification of HMVEC-d seeded into silk microtube lumen (green=VE-cadherin; blue=nuclei; scale bar=50  $\mu$ m). (C) Statistical analysis of collected platelets after perfusion of silk microtubes in presence of endothelium or functionalized with VEGF and VCAM-1 with respect to silk microtube functionalized with ECM components only (average $\pm$ SD, n=5, \*p<0.05).

**Figure 8. Analysis of *ex vivo* platelet release by Mks differentiated from adult human peripheral blood hematopoietic progenitors.** (A) Confocal microscopy imaging of Mks from one healthy control and two patients within the silk-based bone marrow system. (Ai-iii) Imaging of mature Mks immediately after seeding into the silk sponge (green=CD61; blue=nuclei; scale bar=50  $\mu\text{m}$ ). (Aiv-vi) Mks forming proplatelet through the silk microtube wall (green=CD61; blue=nuclei; scale bar=50  $\mu\text{m}$ ). Arrows indicate proplatelet branching and elongation. Silk fibroin 3D scaffolds were stained with Hoechst 33258 and visualized in blue. (B) Flow cytometry analysis of *ex vivo* produced platelets. Samples were mixed with counting beads in order to quantify the number of CD61<sup>+</sup>CD42b<sup>+</sup> platelets. (C) Comparison of platelet count between *in vivo* and *ex vivo* quantified numbers.

# Figure 1

**A****B****C****D****E****F****G****H**

# Figure 2

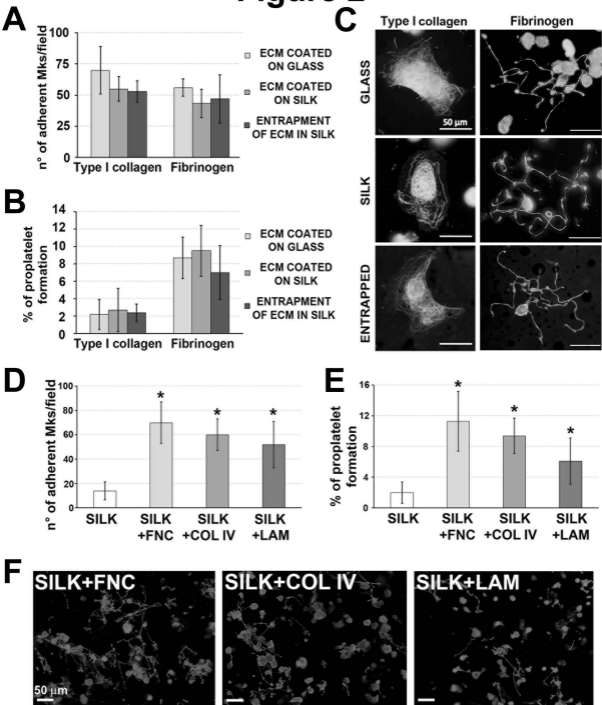


# Figure 3

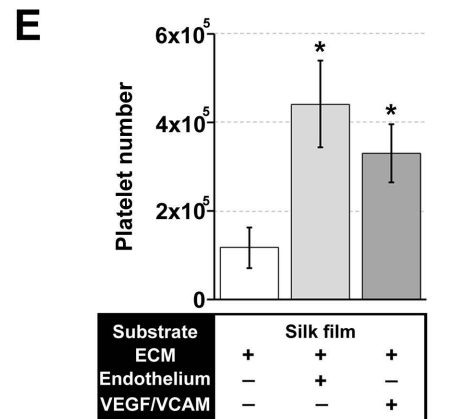
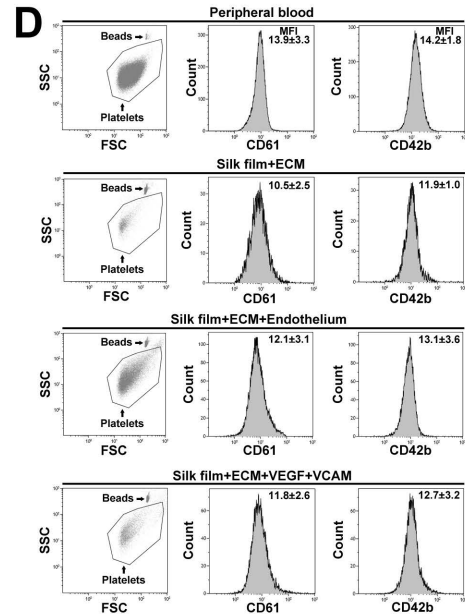
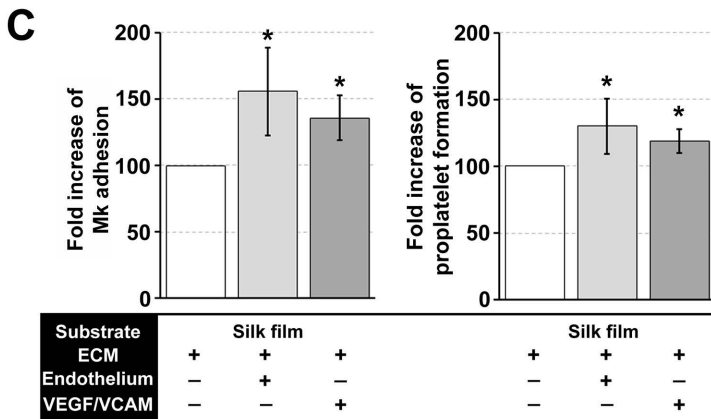
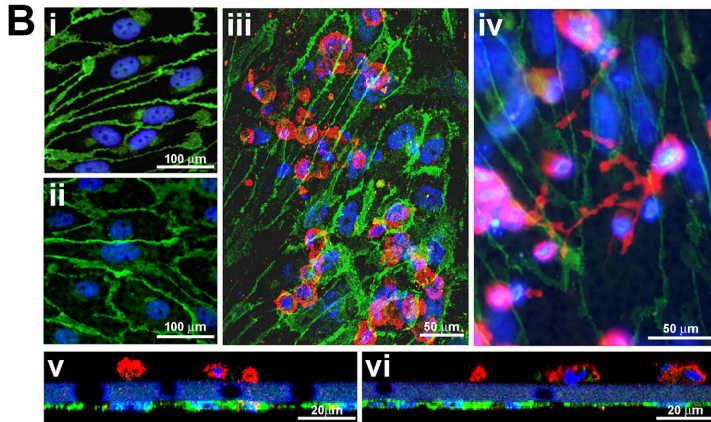
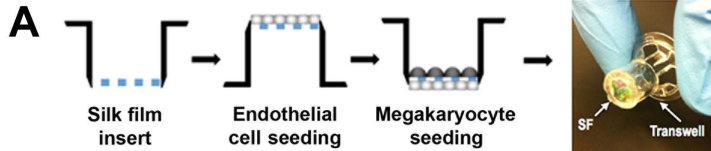
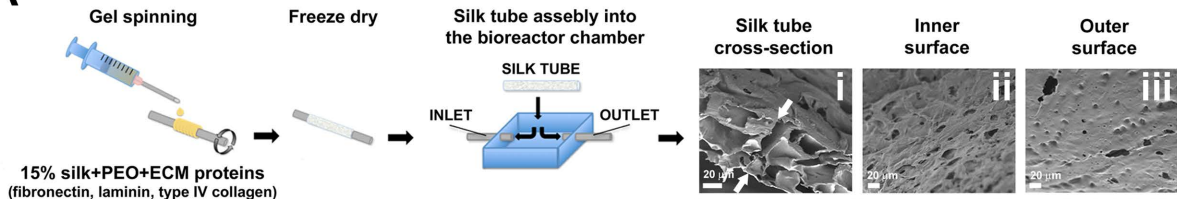


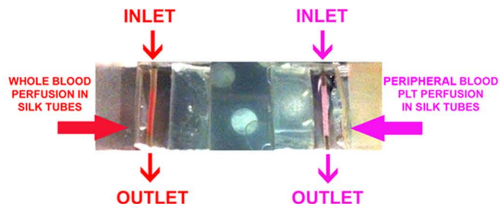


# Figure 4

## A



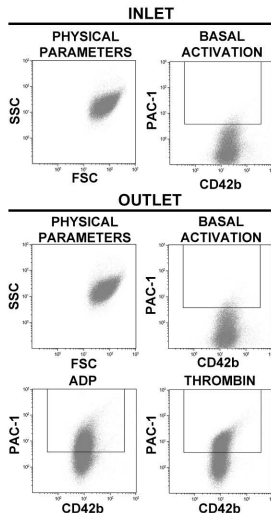
## B



## C

	WBC 10 <sup>3</sup> /μl	RBC 10 <sup>6</sup> /μl	HCT %	MCV fl	MCH pg	MCHC g/dl	RDW %	PLT 10 <sup>3</sup> /μl
<b>INLET</b>	5.7	4.95	42.1	91.5	28.7	31.3	12.4	<b>192</b>
<b>OUTLET</b>	5.3	5.2	41.8	94.5	29.8	31.6	12.9	<b>186</b>

## D



## E

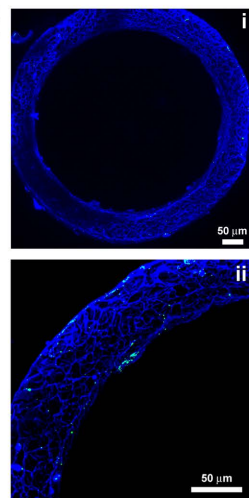


# Figure 5

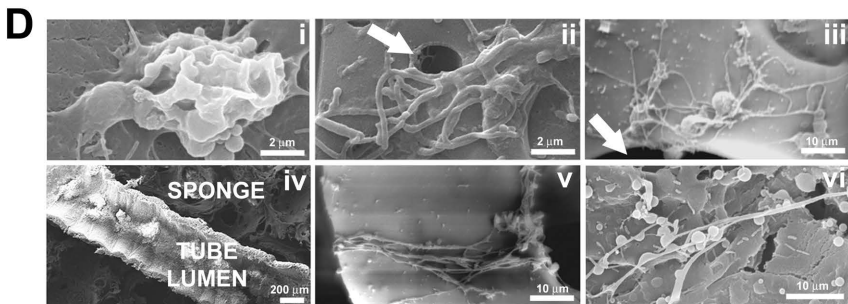
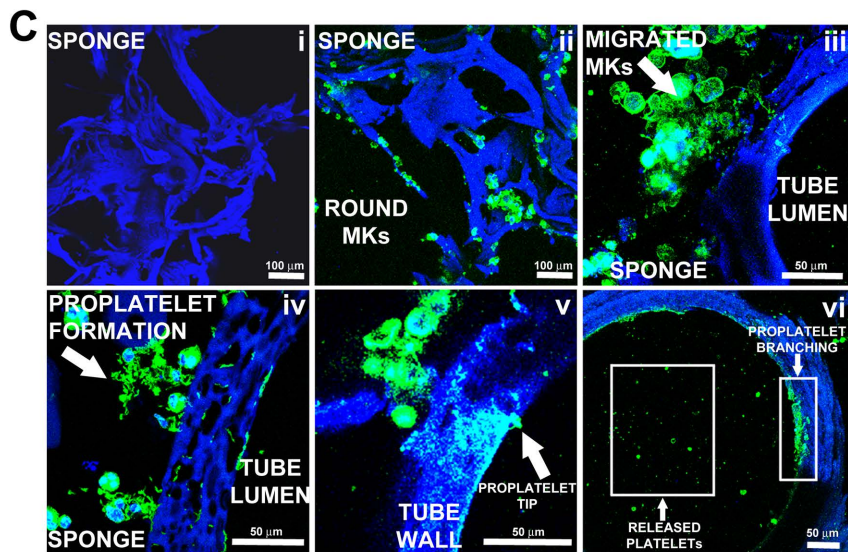
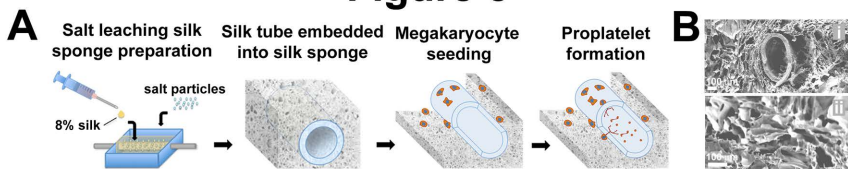


# Figure 6

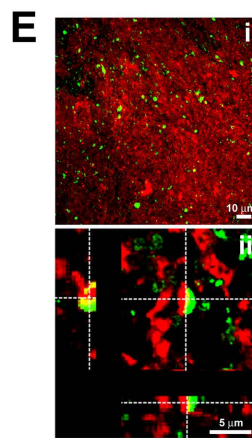
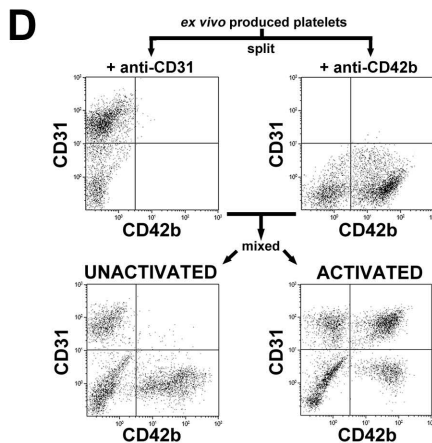
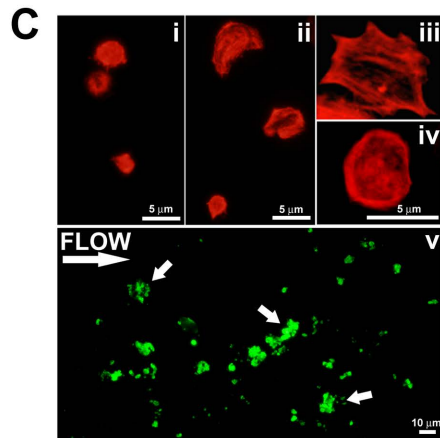
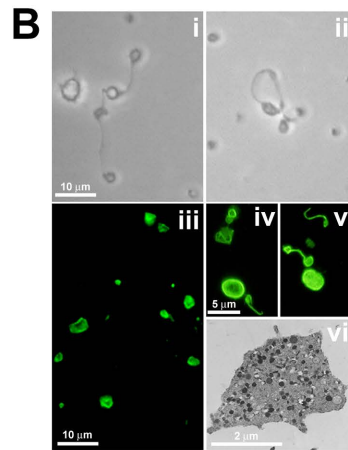
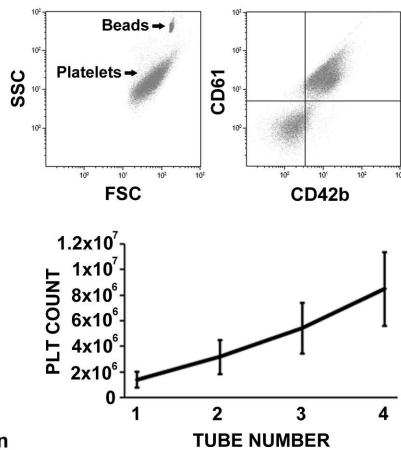
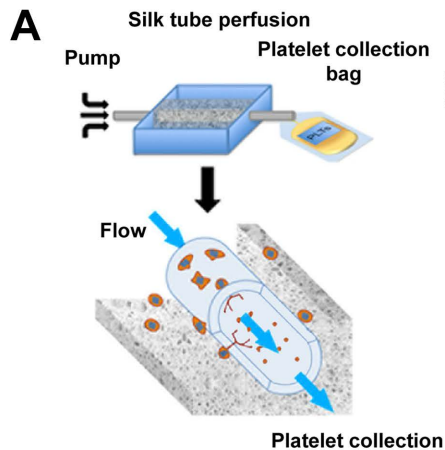
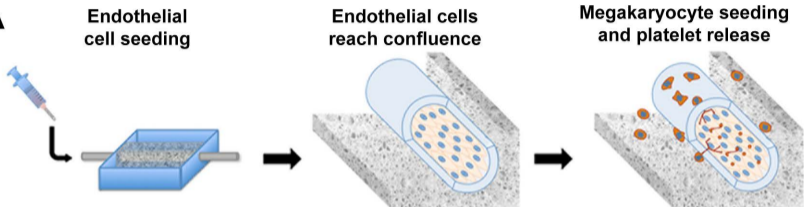
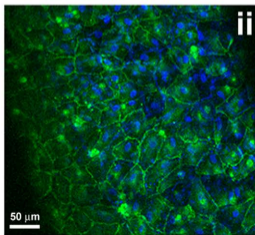
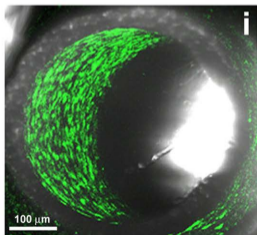


# Figure 7

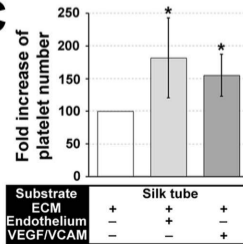
## A



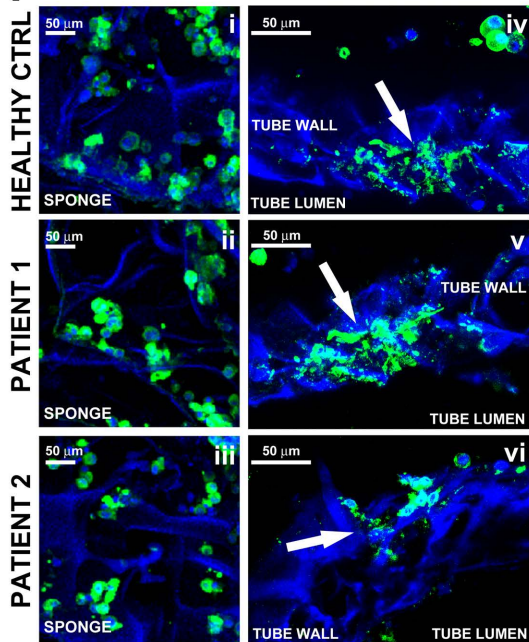
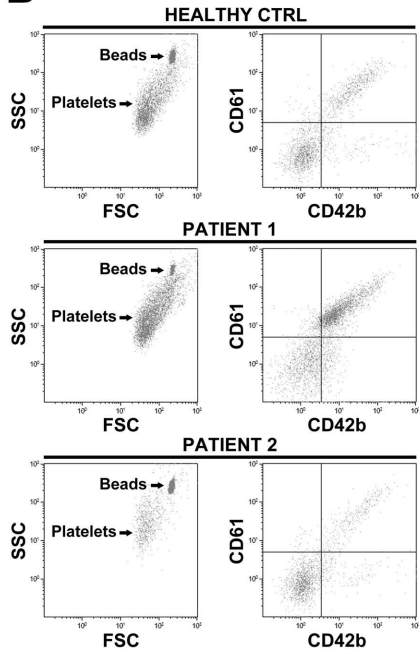
## B



## C



# Figure 8

**A**

**B**

**C**

HEALTHY CTRL	
PLT COUNT	<i>IN VIVO</i> 300x10 <sup>9</sup> /L
	<i>EX VIVO</i> 1.3x10 <sup>6</sup>

PATIENT 1	
PLT COUNT	<i>IN VIVO</i> 430x10 <sup>9</sup> /L
	<i>EX VIVO</i> 2.1x10 <sup>6</sup>

PATIENT 2	
PLT COUNT	<i>IN VIVO</i> 120x10 <sup>9</sup> /L
	<i>EX VIVO</i> 0.5x10 <sup>6</sup>



# blood

Prepublished online January 9, 2015;  
doi:10.1182/blood-2014-08-595561 originally published online  
January 9, 2015

## **Programmable 3D silk bone marrow niche for platelet generation ex vivo and modeling of megakaryopoiesis pathologies**

Christian A. Di Buduo, Lindsay S. Wray, Lorenzo Tozzi, Alessandro Malara, Ying Chen, Chiara E. Ghezzi, Daniel Smoot, Carla Sfara, Antonella Antonelli, Elise Spedden, Giovanna Bruni, Cristian Staii, Luigi De Marco, Mauro Magnani, David L. Kaplan and Alessandra Balduini

---

Information about reproducing this article in parts or in its entirety may be found online at:  
[http://www.bloodjournal.org/site/misc/rights.xhtml#repub\\_requests](http://www.bloodjournal.org/site/misc/rights.xhtml#repub_requests)

Information about ordering reprints may be found online at:  
<http://www.bloodjournal.org/site/misc/rights.xhtml#reprints>

Information about subscriptions and ASH membership may be found online at:  
<http://www.bloodjournal.org/site/subscriptions/index.xhtml>

---

Advance online articles have been peer reviewed and accepted for publication but have not yet appeared in the paper journal (edited, typeset versions may be posted when available prior to final publication). Advance online articles are citable and establish publication priority; they are indexed by PubMed from initial publication. Citations to Advance online articles must include digital object identifier (DOIs) and date of initial publication.